Xiaohong Wang,[1] Haitao Gu,[1] Wei Huang,[2] Jiangtong Peng,[1,3] Yutian Li,[1] Liwang Yang,[1] Dongze Qin,[1] Kobina Essandoh,[1] Yigang Wang,[2] Tianqing Peng,[4] and Guo-Chang Fan[1]

Hsp20-Mediated Activation of Exosome Biogenesis in Cardiomyocytes Improves Cardiac Function and Angiogenesis in Diabetic Mice

Diabetes 2016;65:3111–3128 | DOI: 10.2337/db15-1563

Decreased heat shock protein (Hsp) expression in type 1 and type 2 diabetes has been implicated as a primary factor contributing to diabetes-induced organ damage. We recently showed that diabetic cardiomyocytes could release detrimental exosomes, which contain lower levels of Hsp20 than normal ones. To investigate whether such detrimental exosomes could be modified in cardiomyocytes by raising Hsp20 levels to become protective, we used a transgenic (TG) mouse model with cardiac-specific overexpression of Hsp20. TG and control wild-type (WT) mice were injected with streptozotocin (STZ) to induce diabetes. We observed that overexpression of Hsp20 significantly attenuated STZ-caused cardiac dysfunction, hypertrophy, apoptosis, fibrosis, and microvascular rarefaction. Moreover, Hsp20-TG cardiomyocytes exhibited an increased generation/secretion of exosomes by direct interaction of Hsp20 with Tsg101. Of importance, exosomes derived from TG cardiomyocytes encased higher levels of Hsp20, p-Akt, survivin, and SOD1 than WT exosomes and protected against in vitro hyperglycemia-triggered cell death, as well as in vivo STZ-induced cardiac adverse remodeling. Last, blockade of exosome generation by GW4869 remarkably offset Hsp20-mediated cardioprotection in diabetic mice. Our results indicate that elevation of Hsp20 in cardiomyocytes can offer protection in diabetic hearts through the release of instrumental exosomes. Thus, Hsp20-engineered exosomes might be a novel therapeutic agent for diabetic cardiomyopathy.

Heart failure occurring in patients with diabetes and without hypertension and coronary artery disease, also referred to as diabetic cardiomyopathy, is a common complication of diabetes (1). Over the past decades, numerous mediators/factors (e.g., oxidative stress, cardiac inflammation, insufficient myocardial angiogenesis, lipid accumulation, cardiac fibrosis, and cell death) have been identified as contributors to diabetic cardiomyopathy (2). As a matter of fact, the major cause of diabetes-induced cardiomyopathy is actually associated with impairment of endogenous defense mechanisms by which cardiac cells are vulnerable to a hostile environment (3).

Heat shock response is well recognized as a cellular intrinsic defense mechanism (4). Accumulating evidence has demonstrated that loss of heat shock response would result in cellular dysfunction and abnormality (5). By contrast, increased expression of heat shock proteins (Hsps) could protect cells/tissues against various stress stimuli and pathological conditions (6). Nonetheless, the information regarding the protective effects of Hsps in diabetic hearts is mostly limited to Hsp90, Hsp70/Hsp72, and Hsp60 (7–9). Whether members of the small Hsp family (molecular weight <40 kDa) play fundamental roles in diabetic cardiomyopathy remains largely unknown. Reddy et al. (10) recently showed that the expression patterns of various Hsps were differentially regulated in rat hearts under chronic hyperglycemia. Notably, among seven small

[1]Department of Pharmacology and Cell Biophysics, University of Cincinnati College of Medicine, Cincinnati, OH
[2]Department of Pathology and Laboratory Medicine, University of Cincinnati College of Medicine, Cincinnati, OH
[3]Department of Cardiovascular Diseases, Tongji Medical College Union Hospital, Huazhong University of Science and Technology, Wuhan, China
[4]Critical Illness Research, Lawson Health Research Institute, Ontario, Canada
Corresponding author: Guo-Chang Fan, fangg@ucmail.uc.edu.

Received 11 November 2015 and accepted 25 May 2016.

This article contains Supplementary Data online at http://diabetes.diabetesjournals.org/lookup/suppl/doi:10.2337/db15-1563/-/DC1.

X.W. and H.G. contributed equally to this work.

See accompanying article, p. 2829.

Hsps they examined, Hsp20/HspB6 was the only one significantly downregulated in diabetic rat hearts, whereas MKBP/HspB2, HspB3, and αB-crystallin/HspB5 were remarkably upregulated and another three Hsps (Hsp27/HspB1, cvHsp/HspB7, and Hsp22/HspB8) were not altered. These data suggest that *1*) members of the Hsp family may not act redundantly to enable cardiac cells to resist stress conditions and *2*) reduction of Hsp20 may contribute to diabetes-induced cardiac injury. Importantly, our recent study further indicates that diabetic cardiomyocytes contain higher levels of miR-320 than healthy ones, leading to reduced protein levels of Hsp20, a target of miR-320 (11). Thus, the intrinsic protective mechanism may be impaired in cardiomyocytes under diabetic conditions. Most intriguingly, we observed that diabetic cardiomyocytes could spread "disease messages" to their neighboring cells (i.e., endothelial cells) through exosomes, a group of small membrane-bound vesicles secreted by various cell types (11). Therefore, it would be significant to investigate whether overexpression of Hsp20 in cardiomyocytes could protect not only themselves but also neighboring cells via spreading beneficial exosomes within the myocardium under hyperglycemia.

Exosomes are nanometer-sized membrane vesicles (30–100 nm) released by numerous cell types upon fusion of multivesicular bodies (late endosomes) with the cell membrane (12). Of interest, we and others have recently shown that exosomes can induce either deleterious or beneficial effects on cardiac remodeling, depending on the contents enclosed (12–14). For example, miR-223–enriched exosomes secreted by stem cells could attenuate sepsis-induced myocardial inflammation and dysfunction (13). By contrast, circulating exosomes collected from septic patients could trigger dysfunction in endothelial cells and cardiomyocytes through the transfer of NADPH oxidase and nitric oxide synthases (NOS) (14). Importantly, our prior work has indicated that Hsp20 is incorporated into exosomes (15). Hence, as a molecular chaperone, it would be reasonable to speculate that Hsp20 may facilitate loading of other intracellular proteins into exosomes.

In the current study, we used a transgenic (TG) mouse model with cardiac-specific overexpression of Hsp20 and their age-matched wild-type (WT) littermates to induce diabetes by intraperitoneal injection of streptozotocin (STZ). Our results showed that myocardial overexpression of Hsp20 alleviated diabetes-induced cardiac injury. Mechanistically, we identified that elevation of Hsp20 in cardiomyocytes promoted exosome secretion by direct interaction with Tsg101, an initiator of the exosome biogenesis pathway. Furthermore, we discovered that exosomes collected from Hsp20-TG cardiomyocytes encased higher levels of Hsp20, phosphorylated Akt (p-Akt), survivin, and SOD1 and promoted endothelial cell proliferation under in vitro high-glucose (HG) conditions, as well as protected against STZ-induced cardiac adverse remodeling in vivo. Last, inhibition of exosome generation remarkably offset Hsp20-mediated cardioprotection in diabetic mice. Together, our study for the first time shows that Hsp20 could activate exosome generation/secretion in cardiomyocytes, and such exosomes could elicit autocrine- and paracrine-like protective effects in diabetic hearts.

RESEARCH DESIGN AND METHODS

Animals, STZ-Induced Diabetic Models, and GW4869 Treatment

Generation of a TG mouse model with cardiac-specific overexpression of Hsp20 was described previously (16). Male WT and TG mice (6–8 weeks old, FVB/N) were prepared to induce type 1 diabetes in a mouse model by daily intraperitoneal injection of STZ (Sigma-Aldrich) at a dose of 50 μg/g dissolved in a citrate buffer (0.1 mol/L Na citrate, pH 4.5) for 5 days. Control mice received injections of the same volume of citrate buffer. Plasma glucose levels were measured using a blood glucose monitor (OneTouch Ultra2; LifeScan, Inc.) 2–5 days and 3 months after the last STZ administration. GW4869 (Sigma-Aldrich) was initially dissolved in DMSO to make a stock solution. Diluted GW4869 work solution (final DMSO concentration is 0.005%) was intraperitoneally injected daily into diabetic mice at a dose of 1 μg/g for 5 days. The same volume of 0.005% DMSO buffer was injected as control. All animal experiments were carried out in accordance with the *Guide for the Care and Use of Laboratory Animals* prepared by the National Academy of Sciences and published by the National Institutes of Health and were approved by the University of Cincinnati Animal Care and Use Committee.

Isolation and Culture of Adult Mouse Cardiomyocytes

Adult mouse cardiomyocytes were isolated and cultured, as described previously (17). In brief, mice were anesthetized intraperitoneally using sodium pentobarbital (50 mg/kg), and the adequacy of anesthesia was confirmed by the absence of reflex response to foot squeeze. Subsequently, hearts were rapidly removed and perfused with Krebs Henseleit bicarbonate buffer followed by digestion with liberase blendzyme I (0.25 mg/mL; Roche). Cardiomyocytes were dissociated by teasing the ventricles with forceps, followed by addition of 10% serum and 12.5 μmol/L $CaCl_2$. The concentration of $CaCl_2$ was gradually increased to 1 mmol/L and cells were suspended in the culture medium containing 10 mmol/L of 3-butanedione monoxime. Cardiomyocytes were then seeded on laminin-coated (10 μg/mL) dishes and incubated for 36 h. Subsequently, culture supernatants were collected for isolation of exosomes or directly measuring exosome concentration. For cell survival experiments under hyperglycemia, 2 h after attachment, exosomes (10 μg/mL) were added to cultured cardiomyocytes for 4 h, followed by addition of normal glucose (NG; 5 mmol/L) or HG (25 mmol/L) for 24 h. The viable cardiomyocytes were determined using a CellTiter 96 AQueous One Solution Assay Kit (Promega).

Isolation and Characterizations of Exosomes

Exosomes were isolated according to the method described previously (13). In brief, supernatants of cultured

cardiomyocytes were collected on ice and centrifuged at 3,000 rpm for 20 min to remove any dead cells, followed by centrifugation at 13,000 rpm for 30 min at 4°C to remove any cellular debris. Subsequently, supernatants were collected and filtered through 0.22-μm filters, followed by ultracentrifugation at 120,000*g* (Ti-45 rotor) for 2 h at 4°C to pellet exosomes. The resulting exosome pellet was washed once with PBS. The serum exosomes were isolated using the reagent purchased from Thermo Fisher Scientific. (catalog no. 4478360). The size of exosomes was measured by dynamic light scattering using a particle and molecular size analyzer (Zetasizer Nano ZS; Malvern Instruments) according to the manufacturer's instructions. The quantity of exosomes was determined by the Micro-BCA assay (Pierce, Rockford, IL) for measurement of total protein. Exosome markers (CD63 and CD81) were determined by Western blotting. In addition, the exosome concentrations in cell culture supernatants or mouse sera were measured using CD63 and CD81 exosome quantitation ELISA kits (System Biosciences) or using a commercially available acetylcholinesterase activity assay kit (System Biosciences).

Western Blotting Analysis

Total protein was extracted from mouse hearts, exosomes, or exosome-treated cells with procedures as described in detail elsewhere (4). Equal amounts of protein were subject to SDS-PAGE. The source of antibodies and dilutions used were as follows: rabbit anti-CD63 (sc-15363), rabbit anti-CD81 (sc-9158), and rabbit anti-Tsg101 (Santa Cruz Biotechnology); mouse anti–p-Akt (Ser473), mouse anti-Akt, rabbit anti-survivin, anti-Rab11a, anti-Rab11b, and anti-Rab35 antibodies (Cell Signaling); and rabbit anti-Hsp22, anti-Hsp27, anti-Hsp60, anti-Hsp70, anti-Hsp90, and anti–αB-crystallin (Affinity BioReagents). A primary antibody against Hsp20 was ordered from Fitzgerald. Either α- or β-actin (Sigma-Aldrich) was used as an internal control.

RT-PCR Analysis for Measurement of CD31 and Collagen I/III Expression in Mouse Hearts

Total RNA was extracted from mouse hearts using miRNeasy Mini kit (Qiagen). The NanoDrop 2000 system (Thermo Fisher Scientific) was used to check the concentration and quality of RNA. cDNA was generated by reverse transcription of 2 μg of total RNA using miScript PCR Starter Kit (Qiagen) according to the manufacturer's instruction. RT-PCR was performed using SYBR GreenER qPCR SuperMix (Invitrogen, Carlsbad, CA) in a total volume of 20 μL. The sequences of all primers were synthesized by Integrated DNA Technologies. Full list of primers for CD31, collagen I/III, and GAPDH are included in Supplementary Table 4. GAPDH was used as an internal control. Relative fold change of target gene expression was calculated by using the $2^{-\Delta\Delta Ct}$ method.

Immunostaining Assays

Mice were anesthetized and hearts were arrested in diastole by injection of a cold high-potassium solution (30 mmol/L KCl and 5% dextrose in 1× PBS), followed by retrograde perfusion with PBS to remove any blood. Subsequently, hearts were fixed in 4% paraformaldehyde, dehydrated, embedded in paraffin, and sectioned for the following immunostaining analyses. For myocardial microvascular staining, the slide was rehydrated and boiled to 95°C in 0.01 mol/L sodium citrate solution (pH 6.0). After cool down to room temperature, the slide was balanced with PBLEC solution (PBS + 0.01 mol/L $CaCl_2$, $MgCl_2$, $MnCl_2$, pH 6.8) and stained with isolectin B4 (iB4; Invitrogen) overnight. For detection of cardiomyocyte size, heart sections were stained with a fluorescence Oregon Green 488–labeled wheat germ agglutinin (WGA; Invitrogen). Immunostaining images were obtained using an Olympus BX41 fluorescence microscope (Olympus America, Melville, NY) at ×200 magnification and evaluated using ImageJ software. Microvascular density was detected at low magnification (×200) and calculated at least eight fields randomly selected from each heart section. Myocardial apoptosis assay was performed using the DeadEnd Fluorometric TUNEL system (Promega), followed by staining with an anti–α-sarcomeric actin antibody (Sigma-Aldrich) for cardiomyocytes and DAPI (Invitrogen) for nuclei, as previously described (13). TUNEL-positive myocytes were detected and counted in 10 random fields per heart section. The calculation was expressed as per thousands of the total cardiomyocytes.

Protein-Protein Interaction Assays

Interaction of Hsp20 with proteins involved in the exosome biogenesis/release was determined using competitive binding ELISA assay, as described previously (15). Recombinant human proteins Rab11a (MBS144036; BioSource), Rab11b (H00009230-Q01; Abnova), Rab35 (MBS204753; BioSource), Tsg101 (MBS144073; BioSource), and control protein (BSA) were used. Hsp20-Tsg101 interaction was further confirmed in hearts by coimmunoprecipitation (16).

Cardiac Endothelial Cell Proliferation, Migration, and Tube Formation Assays

A mouse cardiac endothelial cell (MCEC) line was purchased from CELLutions Biosystems. The assessment of MCEC proliferation was performed using an MTS assay (CellTiter 96 AQueous One Solution Assay Kit), per the manufacturer's instructions. In brief, MCECs were seeded in serum-depleted culture medium on 96-well plates at an initial density of 5×10^3 cells/well. After 2 h, exosomes were added at 10 μg/mL for 4 h, followed by the addition of NG (5.5 mmol/L) or HG (25.5 mmol/L) for 24 h. Last, 20 μL MTS/100 μL culture volume was added to measure the cell proliferation with a microplate reader. MCEC migration was evaluated using a Boyden chamber transwell system (BD Biosciences) with the upper chamber having a 8-μm pore size membrane, in which MCECs were plated (4×10^4 cells/well). WT or TG exosomes (WT-Exo or TG-Exo) at 10 μg/mL were added to the culture medium. After 12 h of incubation, cells were fixed and stained with hematoxylin (Sigma-Aldrich) for 10 min, and the upper surface of transwell chambers was wiped with a cotton swab. Migrating cells were counted in

five random microscopic fields (×200). The formation of capillary-like structures was assessed in a 12-well plate using a growth factor–reduced Matrigel (BD Biosciences), per the manufacturer's instructions. For this procedure, MCECs were treated with exosomes (10 μg/mL) for 4–6 h. Subsequently, MCECs were collected and seeded (3×10^4 cells/well) on top of Matrigel (400 μL/well). After 6 h, cells were fixed in 70% ethanol and photos were taken under an inverted light microscope at ×200 magnification. Total capillary tube lengths and tube branch points were quantified using the software Image-Pro Plus 5.1. Five independent fields were assessed for each well, and the average number of tubes was calculated.

Exosome Labeling for In Vitro and In Vivo Detection

For in vitro detection, exosomes were labeled with a PKH67 green fluorescent dye (Sigma-Aldrich) at a dilution of 1:200, according to the manufacturer's instructions. In brief, the exosomal pellet was resuspended in 1 mL PKH67 solution and incubated for 10 min. After ultracentrifugation at 120,000*g* for 70 min at 4°C, the exosomal pellet was washed once in PBS, followed by centrifugation for 90 min at 120,000*g* to remove free dye. Then the pellet was resuspended in 500 μL culture medium containing 10% exosome-depleted FBS (System Biosciences). Labeled exosomes were 50-fold diluted and added to MCECs for 4 h. Then, uptake assays were performed under fluorescence microscopy. For in vivo detection, exosomes were labeled with the lipophilic near-infrared red dye DiR (D12731; Invitrogen). DiR dye is ideal for in vivo application owing to its high tissue penetrance and low autofluorescence. The stock solution of DiR was prepared in ethanol. A 300 μmol/L working solution was prepared in Diluent C solution (Sigma-Aldrich). Exosomes isolated from culture supernatant derived from cardiomyocytes were incubated with 2 μmol/L DiR for 30 min. The exosomes were then washed with 10 mL PBS, followed by ultracentrifugation for 90 min at 120,000*g* to remove free dye. The resulting exosomes were resuspended in PBS and injected intravenously into WT mice (1 μg/g). One hour later, mouse hearts were collected and placed in prelabeled base molds filled with frozen tissue matrix. Subsequently, these hearts were snap frozen in liquid nitrogen. Frozen sections of 7 μm were cut and counterstained with Alexa Fluor 488–conjugated anti–α-actin antibody (ab184675; abcam).

Measurement of Reactive Oxygen Species and SOD1 Levels in Cells and Exosomes

The levels of reactive oxygen species (ROS) were measured using an oxidation-sensitive fluorescent probe, CM-H2DCFDA (Invitrogen). The cell lysates were incubated with 10 μmol/L CM-H2DCFDA for 30 min at 37°C. Then, the ROS generation was measured by the fluorescence intensity in each well at an excitation wavelength of 495 nm and an emission wavelength of 530 nm. SOD1 levels in exosomes or exosome-treated cells were assessed using a mouse SOD/SOD ELISA kit (LS-F4235; LifeSpan BioSciences).

Assessment of Cardiac Function In Vivo

Cardiac function was assessed in vivo using *trans*-thoracic M-model echocardiography (Vevo2100 Imaging System; Visualsonics) with a 15-MHz probe, as described previously (13).

Statistical Analysis

Data were expressed as means ± SEM. Differences among groups were determined by one-way or two-way ANOVA followed by the Bonferroni post hoc test using the GraphPad Prism 5 program. Comparisons between two groups were performed by Student *t* test. A value of $P < 0.05$ was considered statistically significant.

RESULTS

Expression Profiles of Hsps in Murine Hearts Under Acute and Chronic Hyperglycemia Conditions

Heat shock response is a fundamental cellular defense action against a variety of physiological, environmental, and pathological stress insults such as hyperglycemic condition, a major cause of diabetic cardiomyopathy (3–5). To determine the expression pattern of Hsps in diabetic hearts, STZ was injected intraperitoneally daily into mice for 5 days to induce hyperglycemic condition (Fig. 1*A*). At 5 days after the last injection, the concentration of blood glucose was dramatically increased, compared with those treated with citrate buffer (Fig. 1*B*). One set of these hyperglycemic (>250 mg/dL) mice were sacrificed to collect hearts for Western blotting. The remaining hyperglycemic mice were kept for 3 months, and these mice exhibited higher blood glucose (average >400 mg/dL) (Fig. 1*B*) and less increase of body weight (Fig. 1*C*) than age-matched controls. The results of Western blotting assays (Fig. 1*D* and *E*) showed that expression levels of Hsp90, Hsp27, and Hsp22 were dramatically upregulated in mouse hearts at 10 days after STZ treatment, whereas there were no alterations at 3 months after STZ injection, comparable with respective controls. Cardiac Hsp70 expression was not changed at 10 days after STZ injection but was remarkably reduced by 49% at 3 months after STZ challenge. Interestingly, the expression of Hsp20 was significantly upregulated by 1.5-fold at 10 days in STZ-treated mouse hearts, whereas it was remarkably reduced by 52% at 3 months after STZ injection, compared with respective controls. Neither Hsp60 nor αB-crystallin was altered in STZ-treated mouse hearts at either 10 days or 3 months. These data indicate that the expression patterns of various Hsps are distinct in the hearts under hyperglycemic conditions. It suggests that these Hsps may not be redundant in providing cardioprotection against diabetes-induced injury.

Myocardial Overexpression of Hsp20 Alleviates Diabetic Cardiomyopathy in Mice

As described above, cardiac Hsp20 was the only one altered in response to both acute and chronic hyperglycemic conditions. We further examined a time course alteration of Hsp20 expression levels in STZ-treated mouse hearts and validated that protein levels of Hsp20 were significantly

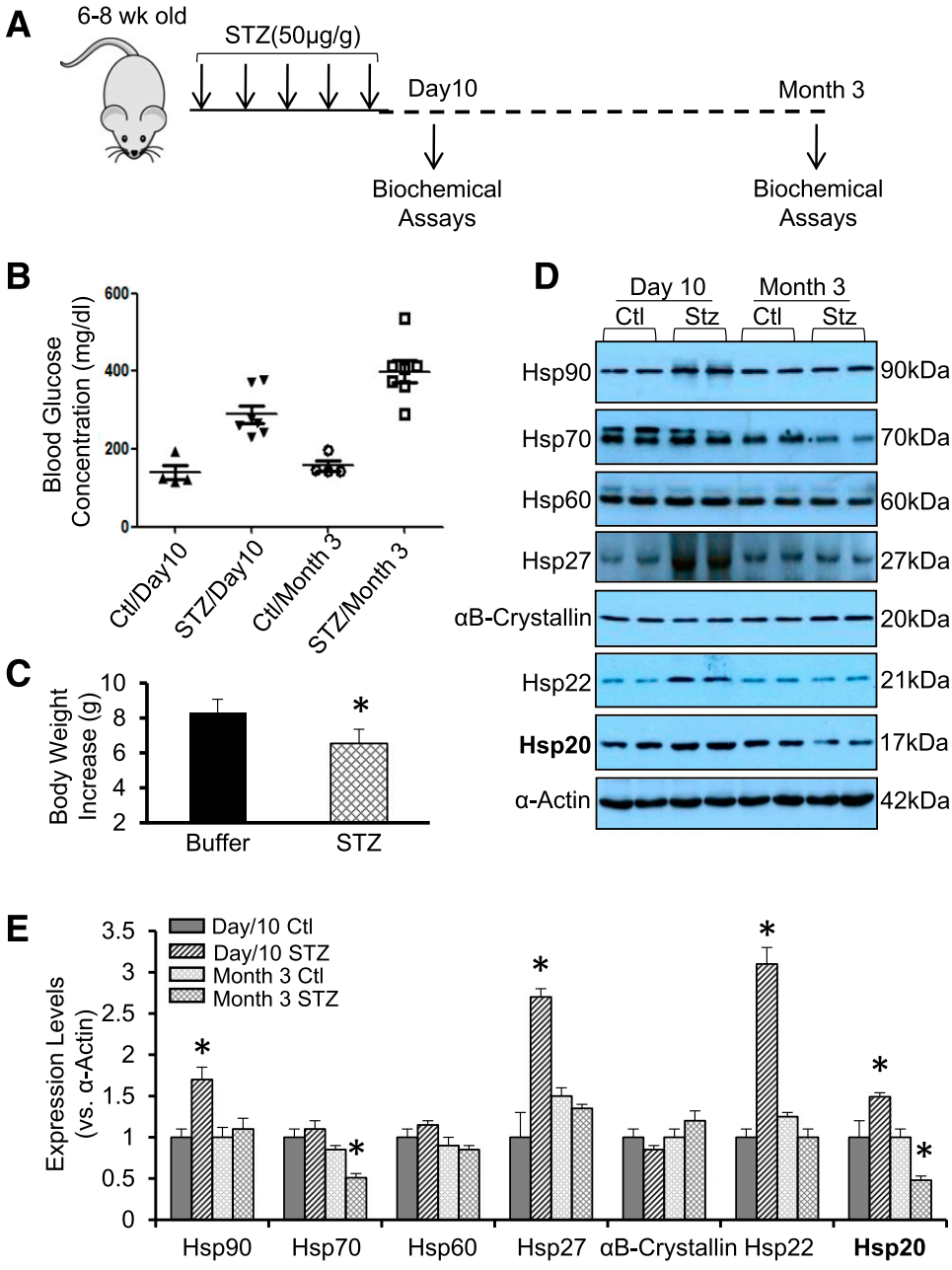

Figure 1—Hsp expression profiles in acute and chronic STZ-treated murine hearts. *A*: A diagram of STZ treatment in mice and sample collection for biochemical assays. *B*: Blood glucose concentration was measured in mice at 10 days or 3 months after the first injection of STZ or buffer. *C*: Body weight increases were measured in mice at 3 months after the first injection of STZ or buffer (n = 4 for buffer-treated group and n = 7 for STZ-treated group). *P < 0.05. Representative Western blots (*D*) and quantitative results (*E*) showed that the distinct expression pattern of various Hsps in acute and chronic STZ-treated mouse hearts. α-Actin was used as a loading control (n = 4). *P < 0.05 vs. controls. Ctl, control; wk, week.

increased in mouse hearts at 10 days post–STZ injection, returned to basal levels at 4 weeks post–STZ injection, and remarkably decreased at 8 weeks and 14 weeks post–STZ treatment (Supplementary Fig. 1). To determine whether cardiac elevation of Hsp20 levels could interfere in diabetes-triggered cardiomyopathy, we used an Hsp20-TG mouse model in which Hsp20 was overexpressed under the control of the cardiac-specific α-myosin heavy chain promoter (16). TG hearts showed a 10-fold increase in total Hsp20 protein compared with WT mouse hearts (Fig. 2*A* and *B*). Six-to-eight-week-old WT and TG were injected intraperitoneally daily with STZ (50 μg/g) or a comparable volume of citrate buffer for 5 days. Throughout the 3-month study period, both WT and TG that received STZ developed severe hyperglycemia and the blood glucose level was similar between the two groups (WT, 437 ± 21 mg/dL; TG, 401 ± 35 mg/dL; n = 11; $P > 0.05$). To investigate the consequence of Hsp20 overexpression on

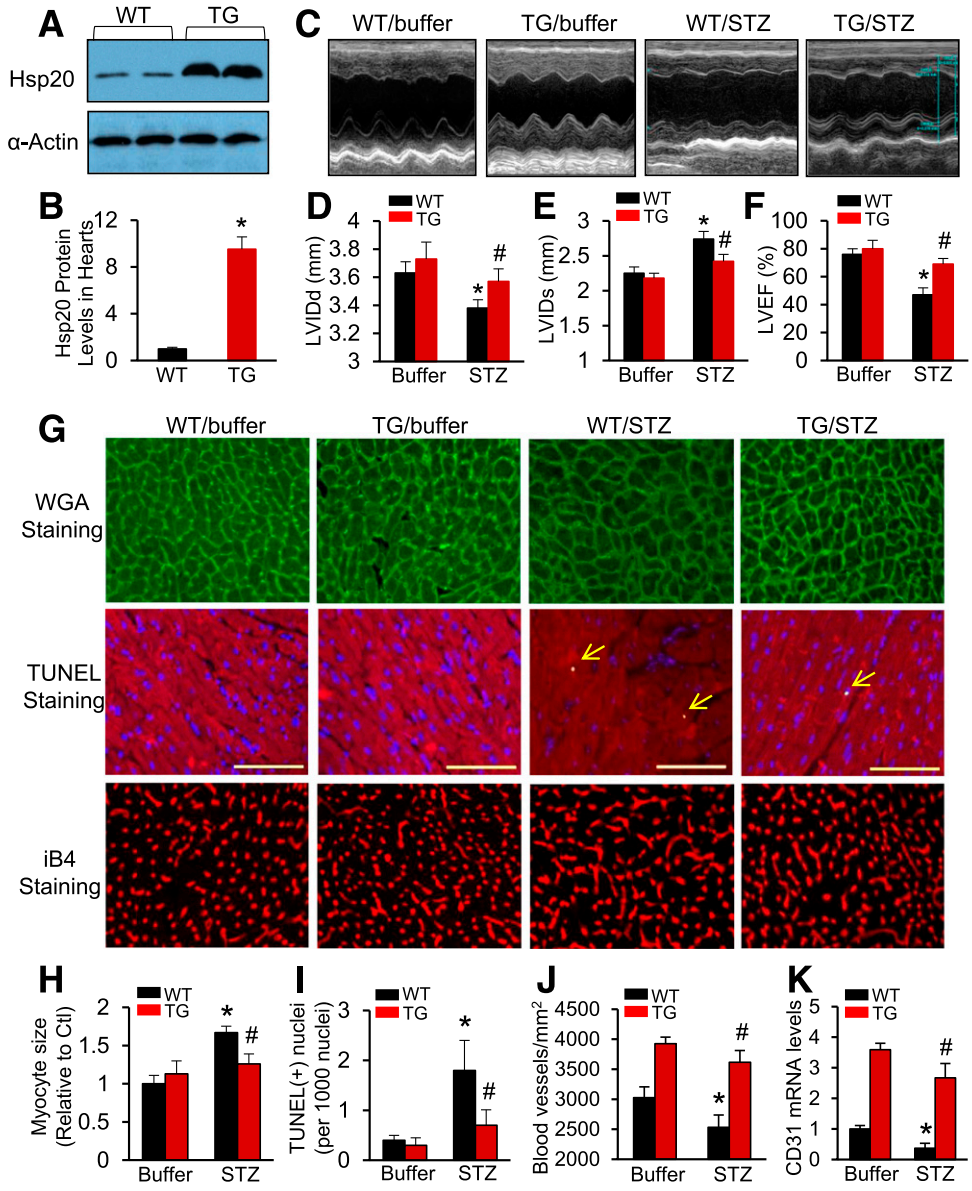

Figure 2—Cardiac-specific overexpression of Hsp20 attenuates STZ-induced cardiac dysfunction and remodeling. *A* and *B*: Western blotting results showed that Hsp20 was overexpressed by 10-fold in TG mouse hearts. α-Actin was used as a loading control ($n = 4$). *$P <$ 0.05 vs. WT. *C–F*: STZ-induced cardiac depression in WT mice, measured by echocardiography (*C*), was significantly improved in Hsp20-TG mice ($n = 5$ for buffer-treated WT or TG group and $n = 9$ for STZ-treated WT or TG). *$P < 0.05$ vs. WT/buffers; #$P < 0.05$ vs. WT/STZ. *G–K*: Hsp20 overexpression protected mice against STZ-induced adverse remodeling. Cardiomyocyte hypertrophy, determined by WGA staining, was exhibited in STZ-treated WT hearts, but not in TG (*G* and *H*). Triple staining with anti–α-sarcomeric actin antibody, DAPI, and TUNEL to determine cardiomyocyte apoptosis in STZ-treated WT or TG hearts (arrows indicate TUNEL-positive nuclei) (*G* and *I*). iB4 staining (*G* and *J*) and RT-PCR analysis of CD31 (*K*) to detect myocardial microvessel density (*F* and *J*) ($n = 5$ hearts, with two sections from each heart). Scale bars: 100 μm. *$P < 0.05$ vs. WT/buffers; #$P < 0.05$ vs. WT/STZ. Ctl, control.

heart function, M-mode echocardiography was used to measure cardiac contractile parameters (Fig. 2*C*). Similar to previous findings (1,2,18), chronic hyperglycemia triggered by STZ dramatically reduced left ventricular internal diameter at end-diastole (LVIDd) (Fig. 2*D*) and increased left ventricular internal diameter at end-systole (LVIDs) (Fig. 2*E*), as well as decreased left ventricular ejection fraction (LVEF %) (Fig. 2*F*) in WT mice, compared with buffer-treated controls. Furthermore, the results of isolated heart function, measured using the Langendorff perfusion apparatus, also showed that rates of contraction (+dP/dt) and relaxation (−dP/dt) were remarkably reduced in STZ-treated WT hearts, compared with buffer-injected controls (Supplementary Fig. 2). However, such STZ-caused myocardial dysfunction was significantly attenuated in Hsp20-TG mice (Fig. 2*D–F*, Supplementary Fig. 2, and Supplementary Table 1).

Given that chronic hyperglycemia can result in adverse cardiac remodeling such as cardiomyocyte hypertrophy,

apoptosis, fibrosis, and reductions in microvessel densities, which contribute to ventricular dysfunction (1,2), we next performed myocardial histological analysis of TG/WT mice subjected to STZ or buffer treatment. Using fluorescence Oregon Green 488–labeled WGA staining, we observed that cardiomyocyte size in cross sections was increased by 1.7-fold in STZ-treated WT, compared with buffer-injected controls ($n = 5$, $P < 0.01$) (Fig. 2*G* and *H*). By contrast, there were no significant increases in the size of Hsp20-TG cardiomyocytes under chronic hyperglycemia, compared with buffer-treated samples (Fig. 2*G* and *H*). Myocardial apoptosis, measured by TUNEL staining, showed that the number of apoptotic cardiomyocytes in STZ-treated WT hearts was 2.6-fold higher than STZ-injected Hsp20-TG hearts (Fig. 2*G* and *I*). RT-PCR analysis for collagen I/III, two markers of fibrosis, revealed that the degree of hyperglycemia-induced myocardial fibrosis was greater in WT hearts than TGs (Supplementary Fig. 3*A* and *B*). Immunostaining of myocardial microvessels and RT-PCR analysis for CD31 expression both indicated that under chronic hyperglycemia, there was no significant decrease in the number of microvessels in TG hearts; whereas it was significantly reduced in STZ-WT hearts, compared with buffer-treated controls (Fig. 2*G*, *J*, and *K*). Put together, these data indicate that increased expression of Hsp20 in hearts could prevent diabetes-caused cardiac injury (i.e., hypertrophy, apoptosis, fibrosis, and microvascular rarefaction), thereby improving myocardial contractile function.

Overexpression of Hsp20 Promotes Exosome Generation by Directly Interacting With Tsg101

In mammalian heart, microvessels are well known to play a critical role in cardiac remodeling under stress/disease conditions (18). Intriguingly, our recent studies have shown that diabetic cardiomyocytes are capable of inhibiting angiogenesis through the release of antiangiogenic exosomes (11). Therefore, to clarify whether the exosome biogenesis/release is influenced in hearts by Hsp20 overexpression, we first examined the expression levels of major factors (i.e., Tsg101, Rab11a, Rab11b, and Rab35) known to be involved in the exosome generation (12) (Fig. 3*A*) in Hsp20-TG hearts. The results of Western blotting showed that the levels of Rab35, Rab11a, Rab11b, and Tsg101 were significantly higher in TG hearts than in WT (Fig. 3*B*), suggesting the exosome biogenesis/release pathway is activated by Hsp20 overexpression. To further validate that Hsp20 stimulates exosome generation in cardiomyocytes, we next isolated cardiomyocytes from adult mice and cultured them overnight for measuring the concentration of exosomes in culture supernatants, using exosome marker (CD63 and CD81) detection ELISA kits. We observed that concentrations of $CD63^+$ exosomes and $CD81^+$ exosomes were both higher in culture supernatants collected from Hsp20-TG cardiomyocytes than those from WT cardiomyocytes (Fig. 3*C* and *D*). In addition, we infected cardiomyocytes isolated from WT adult mice with Ad.Hsp20 to overexpress Hsp20 and measured exosome contents in culture supernatants. Similarly, we observed that exosome levels were dose-dependently increased in culture supernatants of Hsp20-infected cardiomyocytes, compared with control Ad.GFP-infected myocytes (Supplementary Fig. 4*A*). Notably, the degree of cell death was not different between these two groups (Supplementary Fig. 4*B*), suggesting that elevation of Hsp20 levels in cardiomyocytes actively stimulates exosome biogenesis/release.

To dissect the mechanisms by which Hsp20 promotes exosome generation, we next determined whether Hsp20 directly binds those exosome-associated mediators using a competitive protein binding assay (Fig. 3*E*). Recombinant Rab35, Rab11a, Rab11b, and Tsg101 proteins were respectively coated in a high-binding 96-well ELISA plate (20 μg/mL) overnight. The BSA protein was used as a control. Various concentrations of the recombinant Hsp20 protein were added to each well to test the binding affinity. Our results showed that the recombinant Hsp20 protein dose-dependently captured the Tsg101 protein, but not Rab11a/b and Rab35 proteins (Fig. 3*F*), suggesting that Hsp20 has the highest affinity binding to Tsg101 and less affinity to Rab11a/b and Rab35. Furthermore, coimmunoprecipitation of homogenates from WT hearts using the Hsp20 or Tsg101 antibody revealed that Hsp20 did interact with Tsg101 (Fig. 3*G* and *H*). Collectively, these results suggest that increased generation of exosomes from Hsp20-overexpressing cardiomyocytes is associated with direct interaction of Hsp20 with Tsg101, a major factor known to initiate exosome biogenesis.

Exosomes Derived From Hsp20-TG Cardiomyocytes Protect Endothelial Cells and Cardiomyocytes Against HG-Induced Stress Conditions

To further determine the functional role of cardiomyocyte-derived exosomes within hearts, we first purified exosomes from the culture supernatants of TG and WT cardiomyocytes, respectively. The average size of these exosomes was similar between WT-Exo (55.2 nm) (Fig. 4*A*) and TG-Exo (54.9 nm) (Fig. 4*B*). In addition, whereas both WT-Exo and TG-Exo contained similar levels of CD63 and CD81 (Fig. 4*C*), two widely recognized molecular markers for exosomes (11,13), the Hsp20 protein was highly enriched in exosomes derived from Hsp20-TG cardiomyocytes, compared with those from WT cardiomyocytes (Fig. 4*C*). To test whether these cardiomyocyte-originated exosomes have any effects on other cell types in response to hyperglycemia, we added either WT-Exo or TG-Exo to cultured MCECs, followed by the treatment with 25 mmol/L of D-glucose (simulating in vivo hyperglycemia) or 5 mmol/L of D-glucose (simulating a normal level of glucose in the blood). Twenty-four hours later, cell proliferation was measured by MTS assay and revealed that both WT-Exo and TG-Exo could significantly improve MCEC proliferation upon HG insults and, notably, the growth rate was higher in TG-Exo–treated

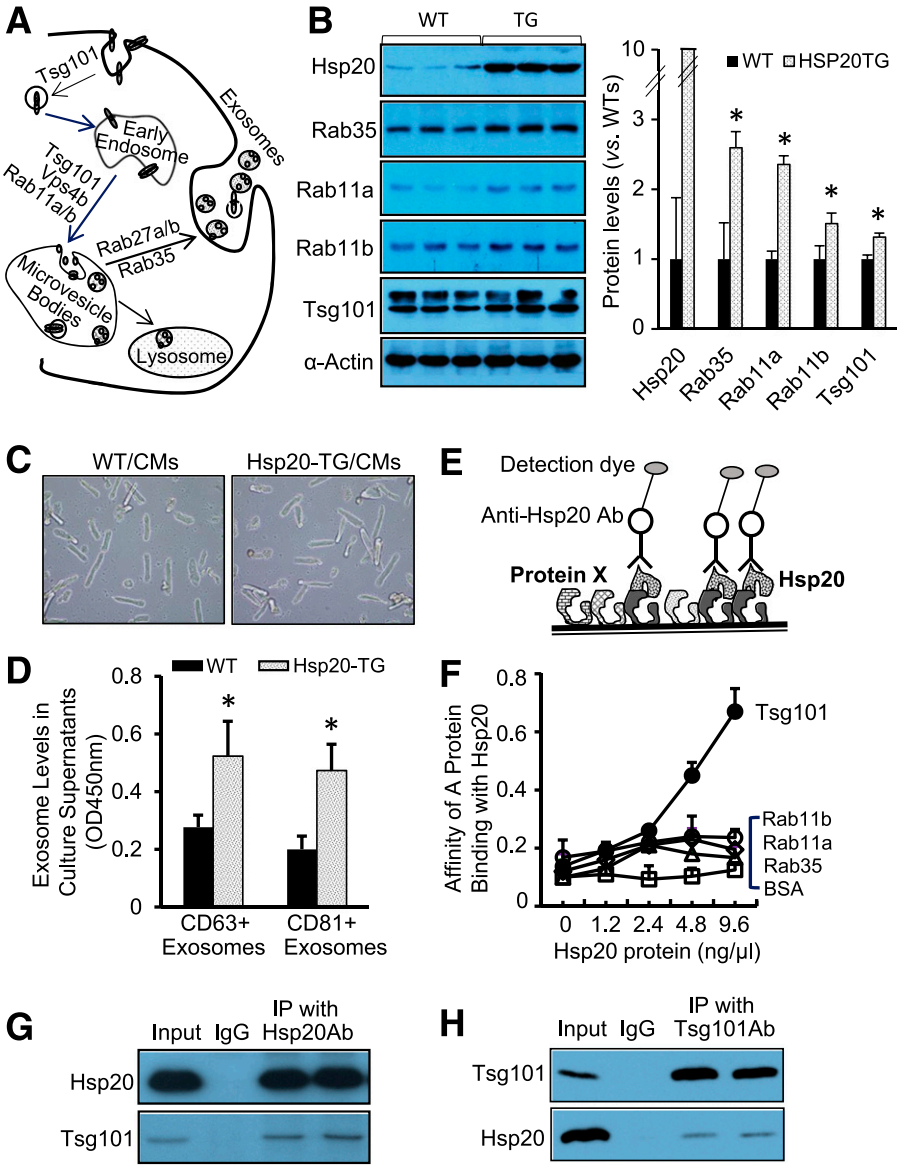

Figure 3—Hsp20 promotes exosome biogenesis via interacting with Tsg101. *A*: Diagram of exosome biogenesis/release pathway. *B*: Overexpression of Hsp20 in the heart increased the expression levels of major mediators involved in exosome generation ($n = 3$). *$P < 0.05$ vs. WT. α-Actin was used as a loading control. *C*: Cardiomyocytes isolated from adult WT or TG mouse hearts were successfully cultured. *D*: The exosome concentration was increased in the culture supernatants of TG cardiomyocytes ($n = 3$ wells). *$P < 0.05$ vs. WT. Similar results were observed from three different hearts. *E*: A scheme for protein-protein interaction analysis. *F*: Recombinant protein Tsg101 coated on a plate dose-dependently captured the Hsp20 protein, whereas Rab11a/b, Rab35, and control protein BSA coated did not effectively arrest the Hsp20 protein. *G* and *H*: Coimmunoprecipitation of heart homogenates with Hsp20 antibody or Tsg101 antibody showed that Hsp20 directly interacted with Tsg101. Ab, antibody; CM, cardiomyocyte; IP, immunoprecipitation; OD, optical density.

MCECs than WT-Exo–treated cells (Fig. 4*D*). We also observed that under NG conditions, MCEC proliferation was greatly promoted by WT-Exo, which was further augmented by TG-Exo, compared with baselines (Fig. 4*D*). Using a transwell assay, we found that WT-Exo increased MCEC migration by 1.3-fold, which was increased by 1.8-fold in TG-Exo–treated cells, compared with controls (Fig. 4*E* and *F*). Accordingly, the tube-like structures were remarkably expanded by the exposure to WT-Exo, which was further enhanced by addition of TG-Exo (Fig. 4*E* and *G*). These results suggest that exosomes released by cardiomyocytes could elicit paracrine-like effects on endothelial cells to a greater degree in Hsp20-TG hearts than WT hearts under hyperglycemia conditions. To determine whether cardiomyocyte-derived exosomes have autocrine-like effects, we isolated cardiomyocytes from adult WT mice and cultured in the presence of either WT-Exo or TG-Exo, followed by the addition of 25 or 5 mmol/L D-glucose. The results of MTS analysis showed that both WT-Exo and TG-Exo

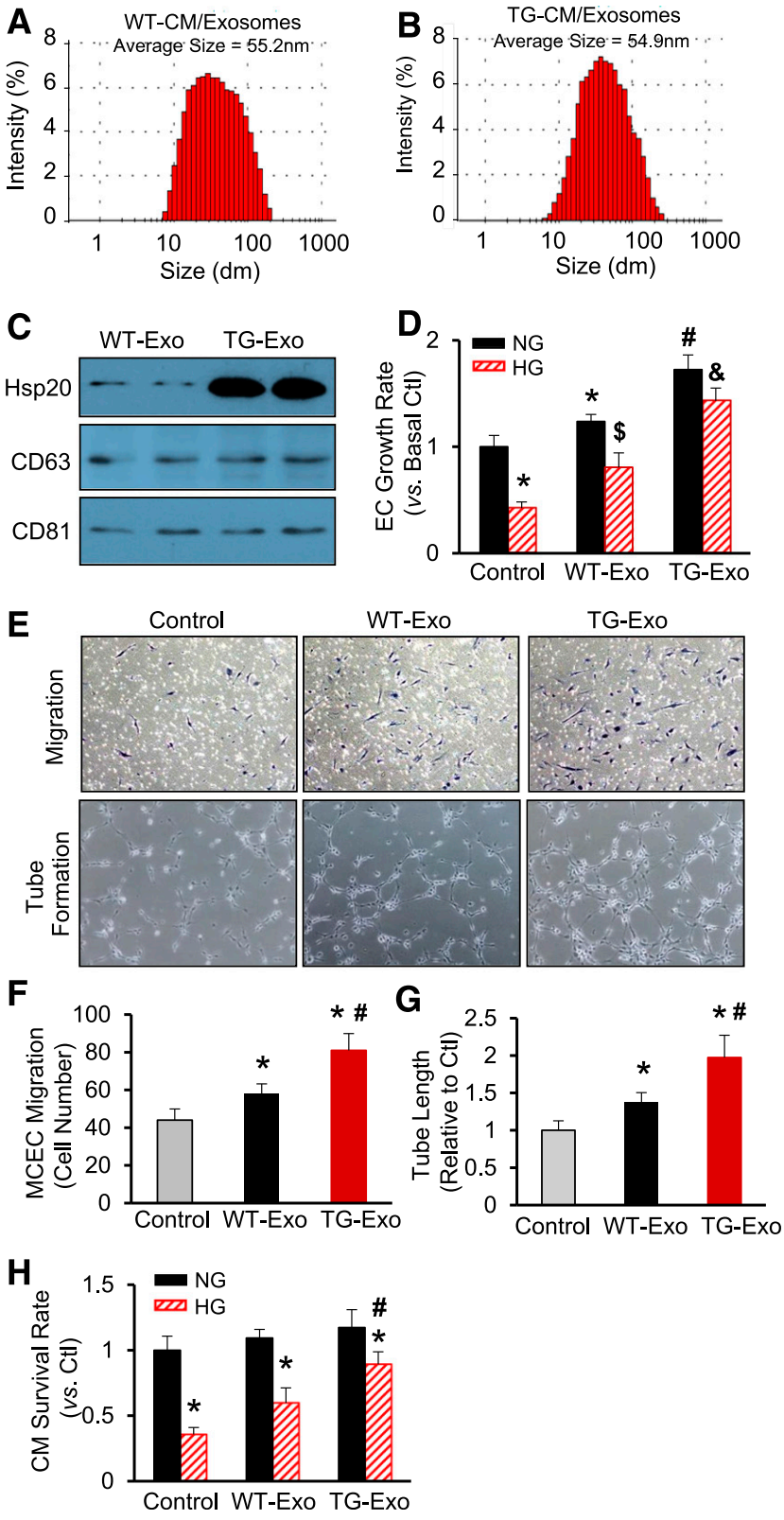

Figure 4—Exosomes derived from Hsp20-overexpressing cardiomyocytes protect myocardial endothelial cells and cardiomyocytes against HG-induced stress conditions. The size of exosomes derived from WT cardiomyocytes (*A*) and Hsp20-TG cardiomyocytes (*B*), measured using a Zetasizer Nano ZS instrument. *C*: Protein levels of CD63 and CD81, two exosome markers, were similarly encased in WT-Exo and TG-Exo. *D*: Effects of WT-Exo (collected from the supernatants of WT cardiomyocytes) and TG-Exo (collected from the supernatants of TG cardiomyocytes) on HG-induced endothelial cell growth ($n = 6$ wells). *$P < 0.05$ vs. control NG conditions; #$P < 0.05$ vs. cells treated with WT-Exo under NG conditions; \$$P < 0.05$ vs. control HG conditions; &$P < 0.05$ vs. cells treated with WT-Exo under HG conditions. Similar results were observed in three additional, independent experiments. Representative endothelial cells that were

significantly increased cardiomyocyte survival upon HG challenge, compared with controls, but the degree of increase was greater in TG-Exo–treated cardiomyocytes than WT-Exo–added cells (Fig. 4*H*). Taken together, these data indicate that Hsp20-overexpressing cardiomyocytes are capable of releasing more powerful and protective exosomes than WT cardiomyocytes and, consequently, protect hearts against hyperglycemia-induced injury.

Hsp20-Modulated Exosomal Contents Can Be Transferred to Other Cell Types

To figure out the mechanisms by which TG-Exo induced better protective effects than WT-Exo, it was necessary to examine protein compositions in these exosomes. After performing the database analysis of published exosomal protein profiles (http://www.exocarta.org), together with the properties of Hsp20 protein, we selected Hsp70, survivin, p-Akt, Akt, and SOD1 for further study. The immunoblotting assay revealed that exosomes released from Hsp20 cardiomyocytes encased higher levels of Hsp20, survivin, and p-Akt than WT-Exo; whereas there were no differences in the levels of Hsp70, total Akt, and exosome markers (CD63 and CD81) (Fig. 5*A* and *B*). The results of ELISA assay showed that the contents of SOD1 were 1.3-fold higher in Hsp20-TG exosomes, compared with WT-Exo (Fig. 5*C*). These data suggest that Hsp20, as molecular chaperone, may facilitate intracellular protein transport to exosomes. Thus, overexpression of Hsp20 in cardiomyocytes may reprogram the exosomal protein contents.

To test whether such a protective message would be spread out within the heart through exosomes, we next labeled exosomes with the green fluorescent membrane dye PKH67 and then incubated them with MCECs or adult mouse cardiomyocytes. Four hours later, we observed that the majority of endothelial cells and cardiomyocytes acquired the green dye–labeled exosomes (Fig. 5*D* and Supplementary Fig. 5*A* and *B*). Accordingly, Western blotting results showed that treatment of MCECs with WT-Exo caused a 1.4-fold increase in the levels of Hsp20 protein, which was remarkably elevated by twofold in TG-Exo–treated cells, compared with controls (Fig. 5*E* and *F*). Similarly, the protein levels of p-Akt and survivin were higher in WT-Exo/MCECs and highest in TG-Exo/MCECs than control cells (Fig. 5*E* and *F*). Consistent with the above observations in MCECs, such exosomal Hsp20, p-Akt, and survivin were also efficiently taken up by cardiomyocytes (Supplementary Fig. 5*C* and *D*).

Hsp20-Enriched Exosomes Dampen HG-Caused Oxidative Stress in Endothelial Cells and Cardiomyocytes

The above data showed that several antioxidant proteins (i.e., SOD1, p-Akt, and survivin) were encased in cardiomyocyte-derived exosomes, we therefore investigated whether WT-Exo and TG-Exo exert antioxidant effects in endothelial cells and cardiomyocytes under HG conditions. Compared with baseline conditions, SOD1 levels were increased by 1.2-fold in MCECs/WT-Exo, and further increased by 1.8-fold in MCECs/TG-Exo (Fig. 6*A*). Remarkably, HG reduced SOD1 levels by 40% in MCECs, which is consistent with previous reports (19). However, such a reduction was significantly attenuated in WT-Exo–treated cells, whereas there was no significant decrease in TG-Exo–treated MCECs in response to HG conditions (Fig. 6*A*). Similar findings were observed in these exosome-treated cardiomyocytes (Fig. 6*B*). Interestingly, we noticed that cardiomyocytes themselves contained higher levels of SOD1 (36.8 $\pm$ 2.9 units/mg) than endothelial cells (12.5 $\pm$ 0.9 units/mg) (Fig. 6*A* and *B*). Moreover, we found that HG dramatically elevated ROS levels by 4.3-fold in MCECs, and such an increase was significantly suppressed by addition of either WT-exo or TG-Exo, but the degree of inhibition was greater in TG-Exo/MCECs than WT-Exo/MCECs (Fig. 6*C*). A similar pattern of ROS alterations was observed in cardiomyocytes treated with WT-Exo or TG-Exo, followed by addition of HG to the culture medium (Fig. 6*D*). Together, these data indicate that exosomes released from Hsp20-overexpressing cardiomyocytes exert antioxidative effects to a greater degree than those derived from WT cardiomyocytes.

Blockade of Exosome Generation Negates Hsp20-Mediated Cardiovascular Protective Effects in Diabetic Mice

To determine whether the cardiovascular protection exhibited in Hsp20-overexpressing hearts is associated with increased generation of exosomes in vivo, we used GW4869, a pharmacological compound known to effectively inhibit exosome biogenesis/release in vivo (20–22). Six-week-old male mice were injected with STZ to induce diabetes, as described above. Seven days later, the mice with high blood glucose (>250 mg/dL) and control mice were administered GW4869 (1 μg/g) or the same volume of DMSO (0.005%) daily five times (Fig. 7*A*). The inhibitory effects of GW4869 on the exosome generation in mice were validated by measuring the total circulating exosome levels at 3 days after the last injection of GW4869. We noticed that under basal condition, circulating exosome

transwelled and formed tube-like structure when exposed to WT-Exo or TG-Exo (*E*) and the quantitative results of migrated endothelial cells (*F*) and tube length formed (G) ($n = 3$ wells). *$P < 0.05$ vs. control; #$P < 0.05$ vs. WT-Exo group. Similar results were observed in three additional, independent experiments. *H*: Effects of WT-Exo and TG-Exo on HG-induced cardiomyocyte death ($n = 3$ wells). *$P < 0.05$ vs. NG conditions; #$P < 0.05$ vs. cells treated with WT-Exo under HG conditions. Similar results were observed in two additional, independent experiments. CM, cardiomyocyte; Ctl, control; dm, diameter; EC, endothelial cell.

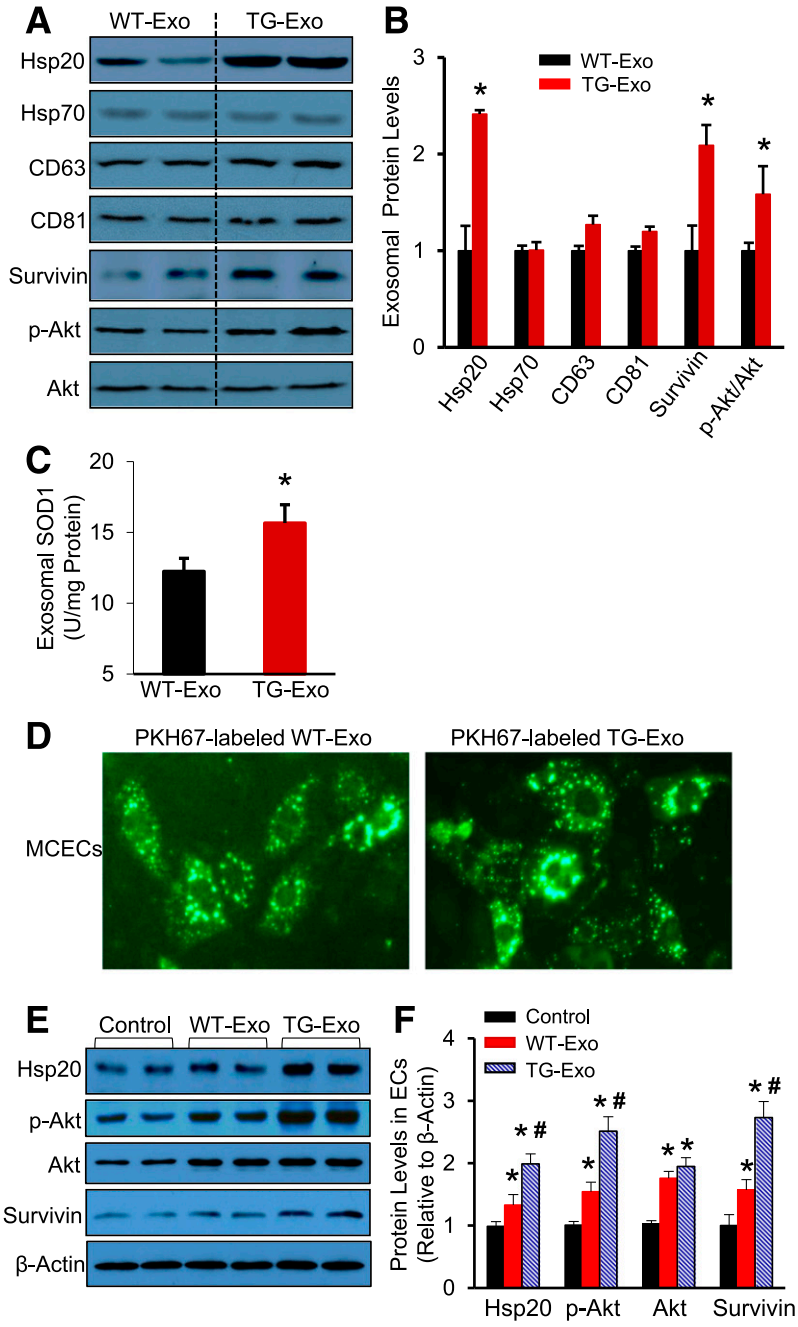

Figure 5—Altered exosomal contents by overexpression of Hsp20 in cardiomyocytes could be delivered to endothelial cells and native cardiomyocytes. Representative Western blots (*A*) and their quantitative results (*B*) showed that higher levels of Hsp20, survivin, and p-Akt encased in TG-Exo than WT-Exo. *C*: SOD1 levels were increased in TG-Exo, compared with WT-Exo ($n = 4$ for *A–C*). *$P < 0.05$ vs. WT-Exo. *D*: Green dye–labeled exosomes were detectable in the cytosol of MCECs after exposure to green dye PKH67-labeled WT- and TG-Exo, respectively. *E* and *F*: Exosomal Hsp20, p-Akt, and survivin were effectively transported to endothelial cells, compared with control conditions ($n = 4$). *$P < 0.05$ vs. control conditions; #$P < 0.05$ vs. WT-Exo–treated samples. β-Actin was used as a loading control. EC, endothelial cell.

levels were higher in Hsp20-TG mice than WT mice ($n = 6$, $P < 0.05$) (Fig. 7*B*), which was correlated with higher serum exosomal Hsp20 levels in TG than WT mice (Supplementary Fig. 6). Given that this TG mouse model is cardiac-specific overexpression of Hsp20, these results may suggest that increased circulating exosomes would be mostly originated from cardiomyocytes. Indeed, our ex vivo data have shown that Hsp20 promoted exosome generation in cardiomyocytes via interacting with Tsg101 (Fig. 3). Three months later, cardiac contractile function measured by echocardiography was significantly improved in Hsp20 diabetic mice under control buffer (0.005% DMSO) treatment, compared with WT diabetic mice (Fig. 7*C–E* and Supplementary Table 2). However, inhibition of

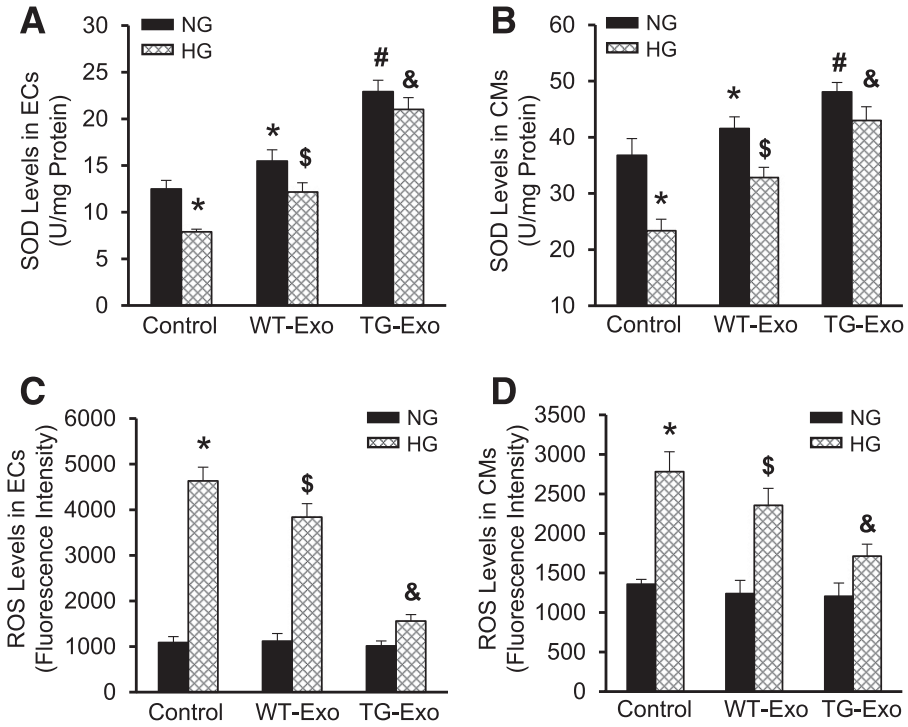

Figure 6—Hsp20 exosomes suppress HG-induced oxidative stress in endothelial cells and cardiomyocytes. The amount of SOD1 was increased in exosome-treated endothelial cells (*A*) and cardiomyocytes (*B*) under normal conditions. HG-induced decrease in the amount of SOD1 was improved to a greater degree in TG-Exo–treated cells than WT-Exo–treated samples (*A* and *B*). By contrast, HG-triggered increase of ROS levels was attenuated to a greater degree in TG-Exo–treated endothelial cells (*C*)/cardiomyocytes (*D*) than WT-Exo–treated samples (*C* and *D*) ($n = 3$ wells). *$P < 0.05$ vs. control NG conditions; #$P < 0.05$ vs. cells treated with WT-Exo under NG conditions; \$$P < 0.05$ vs. control HG conditions; &$P < 0.05$ vs. cells treated with WT-Exo under HG conditions. Data shown are representative of three separate experiments. CM, cardiomyocyte; EC, endothelial cell.

exosome generation by GW4869 impaired Hsp20-mediated improvement of cardiac function in diabetic mice (Fig. 7*C–E* and Supplementary Table 2).

Accordingly, we performed a series of histological analyses of TG/WT diabetic mice subjected to GW4869 or control buffer treatment. As shown in Fig. 7*F* and *G*, whereas the size of cardiomyocytes in Hsp20 diabetc hearts appeared smaller than WT diabetic hearts, GW4869 treatment significantly increased cardiomyocyte size in TG diabetic mice, compared with DMSO-treated TG diabetic mice. Similarly, the number of apoptotic cardiomyocytes in GW4869-treated TG diabetic hearts was twofold higher than DMSO-injected TG diabetic samples (Fig. 7*H* and *I*). Immunostaining (Fig. 7*J* and *K*) and RT-PCR analysis of CD31 expression showed that the density of microvessels was significantly decreased in TG-diabetic hearts upon GW4869 treatment, compared with DMSO-treated controls (Fig. 7*J* and *K* and Supplementary Fig. 7*A*). In addition, RT-PCR analysis of collagen I/III indicated that myocardial fibrosis was significantly augmented in TG diabetic mice by GW4869 treatment, compared with control DMSO buffer injection (Supplementary Fig. 7*B* and *C*). Taken together, these data indicate that Hsp20-induced cardiovascular protective effects were largely offset by GW4869 treatment. It suggests that increased exosome generation from cardiomyocytes contributes to Hsp20-mediated alleviation of cardiac adverse remodeling in diabetic mice.

Exosomes Derived From Hsp20-TG Cardiomyocytes Protect Against STZ-Induced Cardiac Adverse Remodeling In Vivo

Although the above experiments indirectly elucidate the role of exosomes derived from Hsp20-TG cardiomyocytes in diabetic mice, GW4869 may have other actions beyond inhibition of exosome generation/release. Therefore, to further clarify this issue, we performed in vivo experiments to directly test whether Hsp20-incorporating exosomes released from cardiomyocytes elicit protective effects on diabetic mouse hearts. First, we labeled cardiomyocyte-derived exosomes with the near-infrared dye DiR, an ideal red dye for in vivo exosome detection (23,24), and injected them to WT mice via the tail vein. We observed that the entrance of exosomes into cardiomyocytes occurred within 1 h after injection in vivo (Fig. 8*A*). Next, to examine whether Hsp20 could be transferred by cardiomyocyte exosomes in vivo, we injected Hsp20-TG exosomes and WT-Exo into WT mice via the tail vein at different doses (0, 0.5, 1, and 2 μg/g body weight). One hour later, hearts were collected to determine the Hsp20 content. As shown

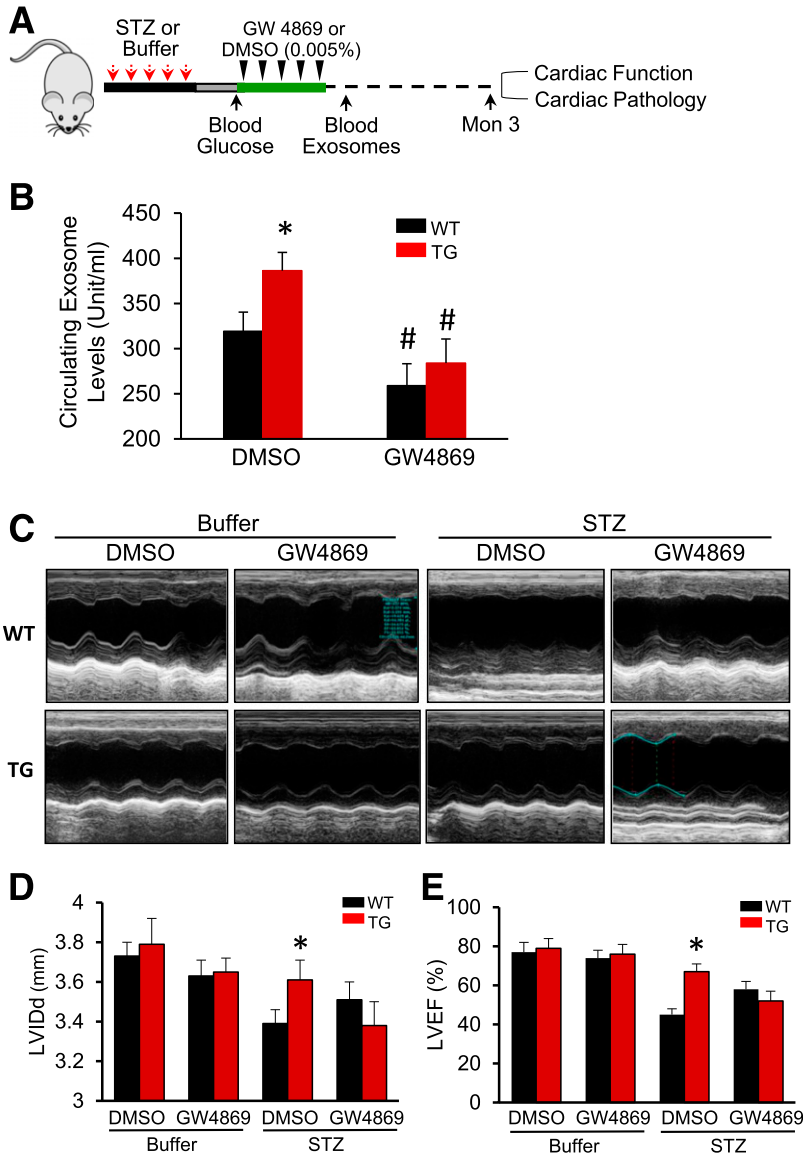

Figure 7—Hsp20-mediated cardioprotective effects are largely offset by blockade of the exosome generation. *A*: A scheme of the experimental procedure for the treatment of mice with STZ and GW4869. *B*: Exosome concentration was measured in the serum of mice treated with GW4869 ($n = 5$). *$P < 0.05$ vs. WT; #$P < 0.001$ vs. DMSO-treated control groups. *C*: Representative echocardiographic images. LVIDd (*D*) and LVEF% (*E*) were calculated in various groups as indicated ($n = 5$ for buffer-treated groups and $n = 7$ for STZ-treated groups). *$P < 0.05$ vs. STZ/DMSO-treated WT. Hsp20-mediated attenuation of cardiomyocyte hypertrophy (*F* and *G*), cardiac apoptosis (*H* and *I*, arrows indicate TUNEL-positive nuclei), and Hsp20-mediated promotion of myocardial angiogenesis (*J* and *K*) were significantly limited by the GW4869 treatment ($n = 5$ hearts, with two sections from each heart). Scale bars: 100 μm. *$P < 0.05$ vs. STZ/DMSO-treated WT. Ctl, control; Mon, month.

in Fig. 8*B* and *C*, the Hsp20 levels were dose-dependently increased in TG-Exo–treated hearts, compared with WT-Exo–injected samples. In addition, we measured the time course protein levels of Hsp20 in TG-Exo–treated mouse hearts and observed that the Hsp20 levels significantly reached peak at 12 h postinjection and then declined at 24 and 48 h postinjection (Fig. 8*D* and *E*). Put together, these data indicate that exogenous TG cardiomyocyte–derived exosomes could effectively deliver Hsp20 protein into murine hearts.

Given our time course and dose-response experimental results (Fig. 8*B*–*E* and Supplementary Fig. 1), we injected TG-Exo or WT-Exo into STZ-induced diabetic mice via the tail vein (1 μg/g) five times at indicated time points (Fig. 8*F*). The same volume of PBS (100 μL) was used as control. Fourteen weeks later, cardiac function was measured by echocardiography and displayed that treatment of diabetic mice with TG-Exo significantly improved myocardial function, compared with WT-Exo–injected and PBS-injected controls (Fig. 8*G* and *H* and Supplementary Table 3). Accordingly, STZ-caused cardiac apoptosis was greatly inhibited in TG exosome–treated hearts, compared with control samples (Fig. 8*I*). Consistent with the in vitro data (Fig. 4*D*–*G*), treatment of diabetic mice with TG-Exo remarkably increased the density of myocardial blood vessels

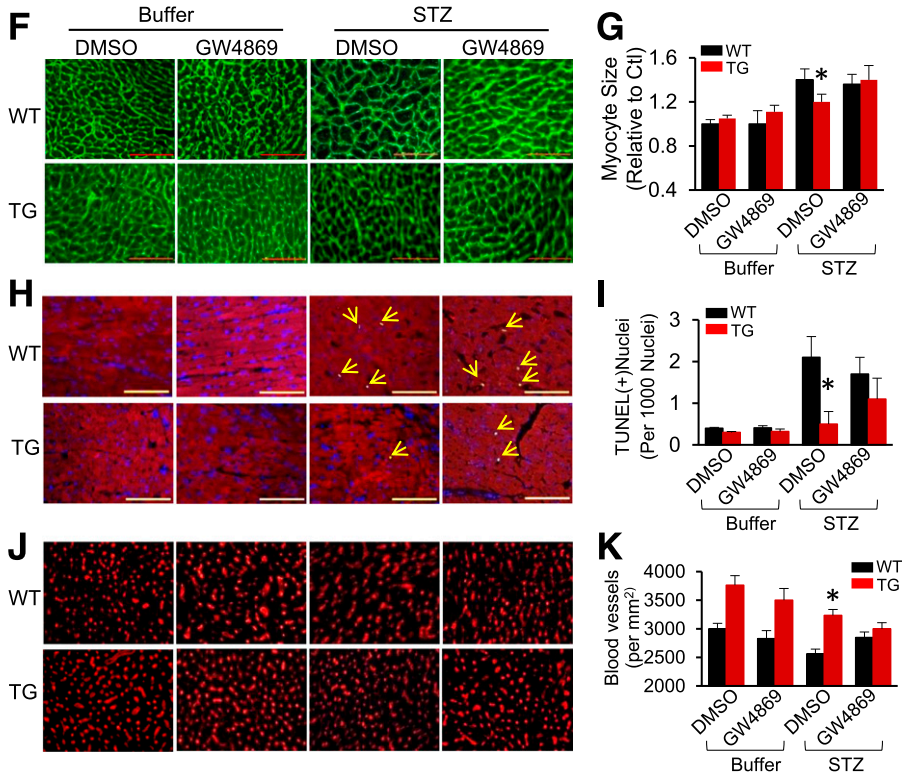

Figure 7—*Continued*.

(Fig. 8*K* and *L*), and further confirmed by RT-PCR analysis for CD31 expression (Fig. 8*M*), compared with WT-Exo– and PBS-treated diabetic hearts. Collectively, these results demonstrate that Hsp20-containing exosomes released from TG cardiomyocytes could elicit protective effects on diabetic mouse hearts.

DISCUSSION

In the current study, we observed that Hsp20 was the only Hsp responsive to both acute and chronic hyperglycemia in mouse hearts, suggesting that decreased Hsp20 in chronic diabetic hearts may be a primary factor leading to the development of diabetic cardiomyopathy. Although our prior work has extensively implicated Hsp20 as an intrinsic protector in the heart under stress or disease conditions (6,16,25,26), whether it has similar protective effects in diabetic hearts remains unknown. Thus, this study for the first time shows that cardiac-specific overexpression of Hsp20 remarkably attenuated diabetes-induced cardiac dysfunction and adverse remodeling. Importantly, we identified that exosomes released from Hsp20-engineered cardiomyocytes elicited paracrine- and autocrine-like protective effects, a novel mechanism underlying Hsp20-mediated protection against diabetes-induced cardiac injury.

Over the past decade, exosomes have been well studied as biomarkers for diagnosis of disease and as a critical tool for cell-to-cell communication (12,27,28). In recent years, it has become clear that exosomes derived from different conditions may contain distinct functional factors (miRNAs/lncRNAs/circRNAs, proteins, etc.) that determine their properties, either detrimental or beneficial (12,28–30). For example, various stem cell–derived exosomes are protective against stress/disease conditions, whereas pathological cells could produce harmful exosomes to spread the disease message (12,13). Our recent work also showed that exosomes released from type 2 diabetic rat cardiomyocytes were capable of inhibiting myocardial endothelial cell proliferation, migration, and tube formation through the transfer of miR-320, a negative regulator of Hsp20 expression (11). Therefore, we were very curious about whether such detrimental exosomes could be reprogrammed to become beneficial ones. In the current study, we excitingly discovered that Hsp20, a chaperone protein, could educate exosomes in cardiomyocytes by shuttling cellular protective proteins (i.e., p-Akt, SOD1, and survivin), together with itself, into exosomes. Remarkably, these exosomal proteins could be delivered to neighboring cells within hearts, leading to reduced oxidative stress, decreased myocardial fibrosis, and apoptosis, as well as increased myocardial angiogenesis; consequently diabetes-induced cardiomyopathy was alleviated. These data suggest that exosomes could be reprogrammed to become protective in cardiomyocytes by overexpression of Hsp20. Hence, our study may provide a novel approach to treatment of diabetic cardiomyopathy by Hsp20-mediated training of cardiomyocyte exosomes.

It is important to mention here that elevation of Hsp20 levels not only modified the contents of cardiomyocyte

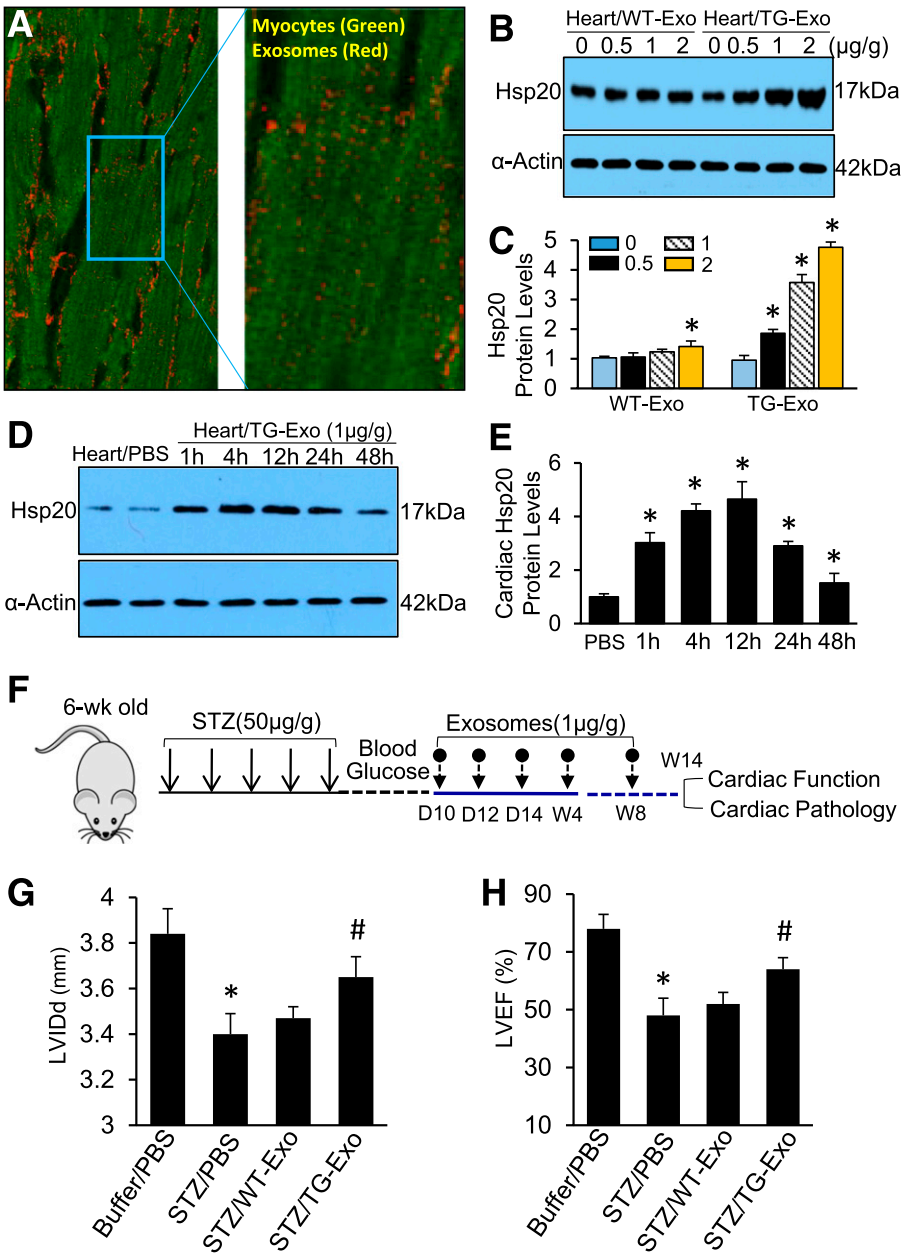

Figure 8—Injection of Hsp20-enriched exosomes collected from TG cardiomyocytes protects mice against STZ-induced cardiac adverse remodeling. *A*: DiR-labeled cardiomyocyte-derived exosomes were detectable in mouse cardiomyocytes 1 h after the tail-vein injection in vivo. The right image is magnified from insert square of *A*. *B* and *C*: Exosomal Hsp20 was dose-dependently delivered to the mouse heart after the tail-vein injection. *D* and *E*: The time course determination of cardiac Hsp20 levels in TG-Exo–injected mice. *F*: A scheme of the experimental procedure for the exosome injection in STZ-treated mice. *G* and *H*: LVIDd and LVEF% were significantly improved in TG-Exo–injected diabetic mice (n = 5–8). *P < 0.05 vs. buffer/PBS group; #P < 0.05 vs. STZ/PBS group. Full echocardiographic data are listed in Supplementary Table 3. *I*: Representative TUNEL staining images (red, α-sarcomeric actin for cardiomyocytes; blue, DAPI for nuclear staining; green, apoptotic nuclear; arrows indicate TUNEL-positive nuclei) and quantification results (*J*) (n = 5 hearts, two sections per heart). *P < 0.05 vs. buffer/PBS group; #P < 0.05 vs. STZ/PBS group. *K*: Representative merged images of WGA staining (cardiomyocytes, green) and iB4 staining (blood vessels, red). *L*: The quantified density of myocardial blood microvessels (n = 5 hearts, two sections per heart, detected at low magnification, ×200) (*L*) and further confirmed by RT-PCR analysis for CD31 expression (n = 5) (*M*). *P < 0.05 vs. buffer/PBS group; #P < 0.05 vs. STZ/PBS group. D, day; W and wk, week.

exosomes but also increased the quantity of exosomes generated in cardiomyocytes. In this study, both in vivo and in vitro evidence consistently showed that overexpression of Hsp20 in cardiomyocytes could enhance the production of exosomes. Mechanistically, we identified that Hsp20 could activate the signaling pathway of cellular exosome generation via directly interacting with Tsg101, an upstream factor of the exosome biogenesis

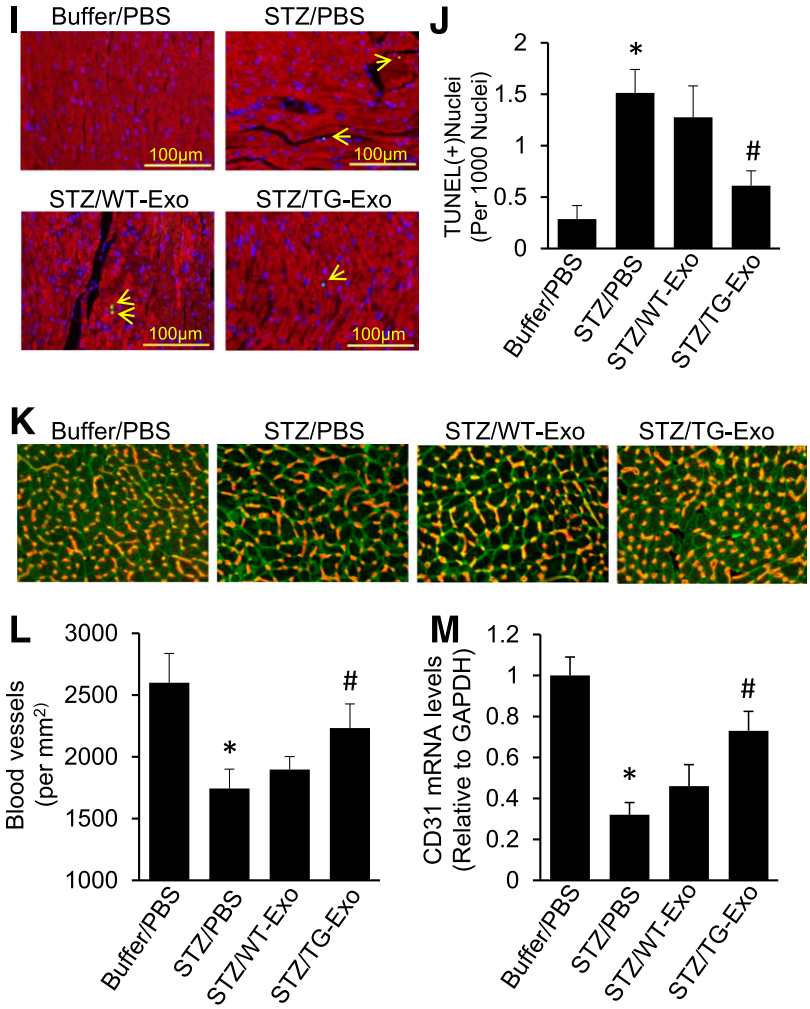

Figure 8—*Continued*.

pathway (12). Considering that heat shock response is a major intrinsic defense mechanism in cells against stress conditions (4–6), our data presented here may provide a new viewpoint that the Hsp-mediated intrinsic protective message could be spread out via exosomes to whole tissue/organ, even whole body.

In addition, we noticed that blockade of exosome generation by GW4869 significantly improved cardiac function in WT diabetic hearts. Indeed, we and others have demonstrated that exosomes released by various types of cells (i.e., peripheral blood mononuclear cells [31], pancreatic β-cells [32], and cardiomyocytes [11]) under hyperglycemic conditions yield a deleterious impact on angiogenesis and cell survival and favor the activation of inflammatory response. For example, Mocharla et al. (31) recently showed that peripheral blood mononuclear cells collected from patients with type 2 diabetes lost their angiogenic capacity due to reduced levels of exosomal miR-126, a proangiogenic miRNA, compared with age- and sex-matched healthy subjects. Recent work by Rahman et al. (32) also showed that exosomes released from the islet cells of nonobese diabetic (NOD) mice could activate autoreactive B and T cells, suggesting that diabetic islet-derived exosomes may function as the autoimmune trigger in NOD mice. In the current study, GW4869 was administered to globally inhibit the biogenesis/release of diabetic exosomes in mice. Therefore, the amelioration of cardiac function observed in GW4869-treated WT diabetic mice may be ascribed to reduced generation of harmful exosomes from multiple types of cells, leading to decreased myocardial fibrosis and increased myocardial angiogenesis. Given that GW4869 is an inhibitor of neutral sphingomyelinase (nSMase) (33), additional protective effects of GW4869 beyond inhibition of exosome biogenesis cannot be excluded. Another limitation for the current study is that adult mouse cardiomyocytes ex vivo could not survive as well as in vivo. Accordingly, the property of exosomes collected from cultured adult mouse cardiomyocytes might not be exactly the same as in vivo myocyte-released exosomes. Therefore, to precisely elucidate the functional roles of exosomes in diabetic cardiomyopathy, future studies using a mouse model with inducible

knockout of cardiac exosomes will be greatly needed. In addition, RNA sequencing and proteomics approaches would be needed to dissect the cardiomyocyte-derived exosomal RNA and protein contents. Nevertheless, GW4869 and ex vivo exosomes used in this study are only for testing whether exosomes are involved in Hsp20-mediated cardioprotection in diabetes.

In summary, the data presented here for the first time demonstrate that elevation of Hsp20 levels in hearts could protect against diabetic cardiomyopathy, which is associated with increased secretion of protective exosomes. Second, we identified that Hsp20 promotes exosome generation in cardiomyocytes through direct interaction with Tsg101, a factor known to activate exosome biogenesis/release. Most significantly, the current study indicates that detrimental exosomes could be reprogrammed in cardiomyocytes by overexpression of Hsp20. Thus, our study may suggest that Hsp20-engineered cells can be either encapsulated to provide sustained local delivery or used as a "factory" to produce protective exosomes, a novel strategy to treat diabetic cardiomyopathy.

Acknowledgments. The authors thank Dr. Lu Cai (University of Louisville, Louisville, KY) for useful suggestions.

Funding. This work was supported by National Institutes of Health grants 2R01-HL-087861 and R01-GM-112930 (to G.-C.F.).

Duality of Interest. No potential conflicts of interest relevant to this article were reported.

Author Contributions. X.W. and H.G. designed and performed the experiments and analyzed the data. W.H. and Y.W. performed the echocardiography analysis. J.P., Y.L., L.Y., D.Q., and K.E. performed the experiments. T.P. contributed reagents and reviewed and edited the manuscript. G.-C.F. conceived and designed the experiments, analyzed the data, and wrote the article. G.-C.F. is the guarantor of this work and, as such, had full access to all the data in the study and takes responsibility for the integrity of the data and the accuracy of the data analysis.

Prior Presentation. Parts of this study were presented in abstract form at the 2014 Scientific Sessions of the American Heart Association, Chicago, IL, 15–19 November 2014, and the 2015 Scientific Sessions of the American Heart Association, Orlando, FL, 7–11 November 2015.

References

1. Gilbert RE, Krum H. Heart failure in diabetes: effects of anti-hyperglycaemic drug therapy. Lancet 2015;385:2107–2117
2. Bugger H, Abel ED. Molecular mechanisms of diabetic cardiomyopathy. Diabetologia 2014;57:660–671
3. Kondo T, Koga S, Matsuyama R, et al. Heat shock response regulates insulin sensitivity and glucose homeostasis: pathophysiological impact and therapeutic potential. Curr Diabetes Rev 2011;7:264–269
4. Richter K, Haslbeck M, Buchner J. The heat shock response: life on the verge of death. Mol Cell 2010;40:253–266
5. Booth LN, Brunet A. Shockingly early: chromatin-mediated loss of the heat shock response. Mol Cell 2015;59:515–516
6. Fan GC, Kranias EG. Small heat shock protein 20 (HspB6) in cardiac hypertrophy and failure. J Mol Cell Cardiol 2011;51:574–577
7. Henstridge DC, Bruce CR, Drew BG, et al. Activating HSP72 in rodent skeletal muscle increases mitochondrial number and oxidative capacity and decreases insulin resistance. Diabetes 2014;63:1881–1894
8. Lei H, Venkatakrishnan A, Yu S, Kazlauskas A. Protein kinase A-dependent translocation of Hsp90 alpha impairs endothelial nitric-oxide synthase activity in high glucose and diabetes. J Biol Chem 2007;282:9364–9371
9. Blasi C, Kim E, Knowlton AA. Improved metabolic control in diabetes, HSP60, and proinflammatory mediators. Autoimmune Dis 2012;2012:346501
10. Reddy VS, Kumar ChU, Raghu G, Reddy GB. Expression and induction of small heat shock proteins in rat heart under chronic hyperglycemic conditions. Arch Biochem Biophys 2014;558:1–9
11. Wang X, Huang W, Liu G, et al. Cardiomyocytes mediate anti-angiogenesis in type 2 diabetic rats through the exosomal transfer of miR-320 into endothelial cells. J Mol Cell Cardiol 2014;74:139–150
12. Ailawadi S, Wang X, Gu H, Fan GC. Pathologic function and therapeutic potential of exosomes in cardiovascular disease. Biochim Biophys Acta 2015;1852:1–11
13. Wang X, Gu H, Qin D, et al. Exosomal miR-223 contributes to mesenchymal stem cell-elicited cardioprotection in polymicrobial sepsis. Sci Rep 2015;5:13721
14. Janiszewski M, Do Carmo AO, Pedro MA, Silva E, Knobel E, Laurindo FR. Platelet-derived exosomes of septic individuals possess proapoptotic NAD(P)H oxidase activity: a novel vascular redox pathway. Crit Care Med 2004;32:818–825
15. Zhang X, Wang X, Zhu H, et al. Hsp20 functions as a novel cardiokine in promoting angiogenesis via activation of VEGFR2. PLoS One 2012;7:e32765
16. Fan GC, Ren X, Qian J, et al. Novel cardioprotective role of a small heat-shock protein, Hsp20, against ischemia/reperfusion injury. Circulation 2005;111:1792–1799
17. Qian J, Vafiadaki E, Florea SM, et al. Small heat shock protein 20 interacts with protein phosphatase-1 and enhances sarcoplasmic reticulum calcium cycling. Circ Res 2011;108:1429–1438
18. Han B, Baliga R, Huang H, Giannone PJ, Bauer JA. Decreased cardiac expression of vascular endothelial growth factor and redox imbalance in murine diabetic cardiomyopathy. Am J Physiol Heart Circ Physiol 2009;297:H829–H835
19. Piconi L, Quagliaro L, Assaloni R, et al. Constant and intermittent high glucose enhances endothelial cell apoptosis through mitochondrial superoxide overproduction. Diabetes Metab Res Rev 2006;22:198–203
20. Li J, Liu K, Liu Y, et al. Exosomes mediate the cell-to-cell transmission of IFN-α-induced antiviral activity. Nat Immunol 2013;14:793–803
21. Kulshreshtha A, Ahmad T, Agrawal A, Ghosh B. Proinflammatory role of epithelial cell-derived exosomes in allergic airway inflammation. J Allergy Clin Immunol 2013;131:1194–1203, 1203.e1–1203.e14
22. Essandoh K, Yang L, Wang X, et al. Blockade of exosome generation with GW4869 dampens the sepsis-induced inflammation and cardiac dysfunction. Biochim Biophys Acta 2015;1852:2362–2371
23. Smyth T, Kullberg M, Malik N, Smith-Jones P, Graner MW, Anchordoquy TJ. Biodistribution and delivery efficiency of unmodified tumor-derived exosomes. J Control Release 2015;199:145–155
24. Ohno S, Takanashi M, Sudo K, et al. Systemically injected exosomes targeted to EGFR deliver antitumor microRNA to breast cancer cells. Mol Ther 2013;21:185–191
25. Wang X, Zingarelli B, O'Connor M, et al. Overexpression of Hsp20 prevents endotoxin-induced myocardial dysfunction and apoptosis via inhibition of NF-kappaB activation. J Mol Cell Cardiol 2009;47:382–390
26. Wang X, Zhao T, Huang W, et al. Hsp20-engineered mesenchymal stem cells are resistant to oxidative stress via enhanced activation of Akt and increased secretion of growth factors. Stem Cells 2009;27:3021–3031
27. Vlassov AV, Magdaleno S, Setterquist R, Conrad R. Exosomes: current knowledge of their composition, biological functions, and diagnostic and therapeutic potentials. Biochim Biophys Acta 2012;1820:940–948
28. Li Y, Zheng Q, Bao C, et al. Circular RNA is enriched and stable in exosomes: a promising biomarker for cancer diagnosis. Cell Res 2015;25:981–984
29. Ibrahim AG, Cheng K, Marbán E. Exosomes as critical agents of cardiac regeneration triggered by cell therapy. Stem Cell Rep 2014;2:606–619

30. Emanueli C, Shearn AI, Angelini GD, Sahoo S. Exosomes and exosomal miRNAs in cardiovascular protection and repair. Vascul Pharmacol 2015;71:24–30

31. Mocharla P, Briand S, Giannotti G, et al. AngiomiR-126 expression and secretion from circulating CD34(+) and CD14(+) PBMCs: role for proangiogenic effects and alterations in type 2 diabetics. Blood 2013;121:226–236

32. Rahman MJ, Regn D, Bashratyan R, Dai YD. Exosomes released by islet-derived mesenchymal stem cells trigger autoimmune responses in NOD mice. Diabetes 2014;63:1008–1020

33. Yuyama K, Sun H, Mitsutake S, Igarashi Y. Sphingolipid-modulated exosome secretion promotes clearance of amyloid-β by microglia. J Biol Chem 2012;287:10977–10989